

Gas, Iron and Gravitational Mass in Galaxy Clusters:

The General Lack of Cluster Evolution at $z < 1.0$

Hironori MATSUMOTO,¹ Takeshi Go TSURU,²

Yasushi FUKAZAWA,³ Makoto HATTORI,⁴ and David S. DAVIS¹

¹ *Center for Space Research, Massachusetts Institute of Technology,*

77 Massachusetts Avenue, Cambridge, MA02139-4307, USA

E-mail(HM): matumoto@space.mit.edu

² *Department of Physics, Faculty of Science, Kyoto University,*

Sakyo-ku, Kyoto 606-8502

³ *Department of Physics, Graduate School of Science, The University of Tokyo,*

7-3-1 Hongou, Bunkyo-ku, Tokyo 113-0033

⁴ *Astronomical Institute, Tohoku University, Aoba Aramaki, Sendai 980-8578*

(Received ; accepted)

Abstract

We have analyzed the ASCA data of 29 nearby clusters of galaxies systematically, and obtained temperatures, iron abundances, and X-ray luminosities of their intracluster medium (ICM). We also estimate ICM mass using the β model, and then evaluate iron mass contained in the ICM and derive the total gravitating mass. This gives the largest and most homogeneous information about the ICM derived only by the ASCA data. We compare these values with those of distant clusters whose temperatures, abundances, and luminosities were also measured with ASCA, and find no clear evidence of evolution for the clusters at $z < 1.0$. Only the most distant cluster at $z = 1.0$, AXJ2019.3+1127, has anomalously high iron abundance, but its iron mass in the ICM may be among normal values for the other clusters, because the ICM mass may be smaller than the other clusters. This may suggest a hint of evolution of clusters at $z \sim 1.0$.

Key words: Galaxies: clusters of — Cosmology — X-rays: spectra

1. Introduction

Clusters of galaxies are the largest bound systems in the universe and a major fraction of their visible mass is X-ray emitting hot gas which is known as the intracluster medium (ICM). The physical conditions of the ICM are largely determined by the nature of the dynamical and chemical evolution and the dark matter distribution of clusters. Accordingly, X-ray studies for structures of clusters and their evolution provide key information for cosmology.

The main purpose of this paper is to present a large and homogeneous dataset on the temperature, metallicity, luminosity, and density distribution of the ICM in the nearby clusters derived only from the ASCA data (Tanaka et al. 1994). We used the β model to derive the ICM distribution. We then estimated the ICM mass (M_{gas}), the iron mass (M_{Fe}) in the ICM, and the total gravitational mass (M_{tot}) from our results.

Tsuru et al. (1996) and Mushotzky and Scharf (1997) compiled a catalogue using the ASCA data of distant clusters (mostly $0.1 < z < 0.6$), and compared it with the data from nearby clusters obtained with the Einstein and ROSAT observatories (e.g. David et al. 1993). They suggested that no systematic differences exist in the X-ray luminosity (L_X) – temperature (kT) relation between distant clusters and nearby clusters. Mushotzky and Loewenstein (1997) compared iron abundances (A_{Fe}) in the ICM of nearby clusters with those of distant clusters, and found no evidence for evolution of A_{Fe} at $z \lesssim 0.3$. Tsuru et al. (1996) along with Mushotzky and Loewenstein (1997) studied the kT – A_{Fe} relation, and concluded that there are no differences between nearby and distant clusters. However, these studies are based on comparison of the results from different instruments (ASCA, ROSAT, Ginga and Einstein), which should be treated carefully unless cross-calibration between these instruments are fully performed. Thus, the other purpose of this paper is to compare the temperatures, metal abundances, and luminosities of nearby clusters with those of distant clusters using only the ASCA data. We also study the evolution of M_{gas} , M_{Fe} , and M_{tot} by comparing these values for nearby clusters with those of distant clusters in the literature.

Throughout this paper, we assume $H_0 = 50$ km/s/Mpc and $q_0 = 0.5$. All errors used in this paper are at 90 % confident level for one interesting parameter except for AXJ2019. The errors for AXJ2019 are at 1 σ level.

2. Data Analysis and Results of Nearby Clusters

We selected the ASCA sample of clusters with redshifts less than 0.1 using the following requirement: the cluster must be reasonably extended so that it is spatially resolved with ASCA, the X-ray flux is high so that we can

constrain the iron abundance, and its morphology is nearly symmetric to exclude any merger or dynamic effects. We made an effort to include clusters with a wide range of gas temperatures. Finally, there are 29 clusters in our sample which are listed in table 1. The average redshift is 0.032. The ASCA data were screened with the standard selection criteria to exclude such data as affected by the South Atlantic Anomaly, Earth occultation, and regions of low geomagnetic rigidity (Fukazawa 1997).

The GIS spectra for each of the nearby clusters was accumulated from a circular region with a radius of 15 arcmin from the cluster center. We did not use the SIS data, because we did not use them for the imaging analysis as discussed below. We believe that the GIS data alone are sufficient to constrain the temperature and iron abundance of the clusters, because the temperatures of our sample clusters are higher than 2 keV and the GIS has higher sensitivity than the SIS in the energy band above 2 keV. Some of the nearby clusters are known to exhibit two-temperature thermal spectra at their central regions (Fukazawa 1997). However, it is rather difficult to distinguish between a single-temperature spectrum and a multi-temperature spectrum if the total count of the spectrum is low. Since the fluxes of distant clusters are inevitably low, it is difficult to find the multi-temperature structure in the X-ray spectrum of the distant clusters. It was confirmed that the X-ray spectra of distant clusters at redshifts higher than 0.1 were well described with the single-temperature thin thermal plasma model (Mushotzky, Loewenstein 1997; Mushotzky, Scharf 1997). Since one of the main purposes of this paper is to systematically compare the ASCA results of the nearby clusters with those of the distant clusters, we fitted all the GIS spectra of the nearby clusters with the single-temperature model (Masai 1984) with a free absorption (N_{H}). In this fitting, we fixed abundance ratios between various elements to the solar ratio ($(\text{Fe}/\text{H})_{\odot} = 4.68 \times 10^{-5}$; Anders, Grevesse 1989). Since our sample of nearby clusters have temperatures higher than 2 keV and we used only the GIS data, the metal abundances were mainly determined by the iron K line. Therefore, we regard the determined abundances as those of iron. We show the results in table 1. As for the X-ray luminosity, we limited the energy range to be 2 – 10 keV in order to exclude possible contamination from the cool component found in some clusters.

We then analyzed the X-ray surface brightness of the nearby clusters using the GIS data. We did not use the SIS data because the clusters extend beyond its field of view. We made azimuthally averaged radial profiles of X-ray counts typically in the 1.8 – 7.1 keV band to minimize contribution from the central cool component. We fitted the profile with the β model taking account of the complex PSF effects of ASCA (e.g. Takahashi et al. 1995). The β

model, $S(r)$, is given by

$$S(r) = S(0) \left[1 + \left(\frac{r}{r_{\text{core}}} \right)^2 \right]^{-3\beta + \frac{1}{2}}, \quad (1)$$

where r is the radius and r_{core} is the core radius. The best-fit β profile can be converted to the proton density profile of the ICM, $n(r)$, which is expressed as

$$n(r) = n(0) \left[1 + \left(\frac{r}{r_{\text{core}}} \right)^2 \right]^{-\frac{3}{2}\beta} \quad (2)$$

(e.g. Sarazin 1986). We then integrated the density profile to estimate the ICM mass within 1 Mpc from the center. Our results are consistent with those derived by the Einstein or ROSAT data (e.g. White et al. 1997; Mohr et al. 1999). The iron mass included in the ICM within 1 Mpc from the center was estimated by using the best-fit iron abundances in table 1. If we assume hydrostatic equilibrium for the ICM and the isothermal ICM distribution of the β model, the total gravitational mass within a radius R , $M(< R)$, is expressed as

$$M(< R) = 3\beta \frac{kTR}{\mu m_p G} \frac{(R/r_{\text{core}})^2}{1 + (R/r_{\text{core}})^2}, \quad (3)$$

where G is the gravitational constant, μ is the mean molecular weight (we assume $\mu = 0.6$), and m_p is the mass of a proton. We estimate the total mass within the 1 Mpc radius using the equation (3), and the results are shown in table 2. Further details of the observations and analysis of the ASCA data of the nearby clusters are found in Fukazawa (1997).

3. Discussion

In this section, we compare our results with other distant clusters in the literature. Most of our sample of distant clusters are from Mushotzky, Scharf (1997) and Mushotzky, Loewenstein (1997). Therefore, we should note that the sample has a strong bias against clusters of $L_X < 10^{45}$ erg/s, as noted by Mushotzky, Scharf (1997). The temperatures, iron abundances, and X-ray luminosities of the distant clusters were determined only by the ASCA data. Unfortunately, the ASCA imaging quality is insufficient to extract the morphological parameters for most of the distant clusters; hence, we use the ICM and total masses derived with the Einstein or ROSAT data from the literature. Otherwise, we used β model parameters derived with the Einstein or ROSAT data in the literature, and we calculated masses by using them. The iron mass in the ICM was calculated by combining the ICM mass derived as mentioned above and the iron abundance determined with ASCA.

Since the ASCA imaging quality is worse than Einstein and ROSAT, the parameters listed in table 2 have generally larger errors than those determined by the Einstein and ROSAT data in other work (White et al. 1997; Mohr et al. 1999). However, they are consistent with each other. Therefore, systematic calibration errors between different instruments for the morphological parameters are less serious than those of spectroscopic parameters, in particular, temperatures and abundances. Our sample for the distant clusters are listed in table 3 with all relevant parameters. We should note that the errors for AXJ2019 is at 1σ level while the others are at 90 % level, because the original paper (Hattori et al. 1997) shows only the 1σ errors.

We show the $kT - L_X$ relation in figure 1. There is no significant difference between $z < 0.1$ and $0.1 < z < 1.0$. Although the clusters at $0.1 < z < 1.0$ show a somewhat flatter slope than the nearby clusters, this is probably due to the selection bias for the distant clusters as already noted by Mushotzky, Scharf (1997). The most distant cluster, AXJ2019 denoted by a star in figure 1, is also consistent with the other clusters.

Figure 2 shows the $kT - M_{\text{gas}}$ relation. No X-ray emission from the ICM in AXJ2019 was detected beyond 0.5 Mpc from the center (Hattori et al. 1997). Therefore, we used the best-fit parameters of the β model and extrapolated to 1 Mpc from the center, and both of these are plotted in figure 2. We found no difference between the clusters at $z < 0.1$ and $0.1 < z < 1.0$. The most distant cluster, AXJ2019, is marginally consistent with the other clusters taking its large errors into account. However, the best-fit values may suggest that the cluster has less gas mass than the other clusters of similar temperatures. The reason why AXJ2019 may have such a low gas mass in spite of its normal luminosity is that the β of AXJ2019 ($\beta \sim 0.9$) is rather larger than the other clusters ($\beta \sim 0.6$).

Figure 3 shows the $kT - A_{\text{Fe}}$ relation. We see no clear differences between the clusters at $z < 0.1$ and $0.1 < z < 1.0$. However, the most distant cluster has an extremely large best-fit abundance. Most of the clusters having dominant galaxies at their centers show cool components in their X-ray spectra from the central regions. The iron abundance of the cool component is often higher than the surrounding ICM (e.g. Fukazawa 1997). Some clusters in our nearby sample have dominant galaxies, and then they tend to show low-temperatures and high-metallicities in our analysis as well. We believe this can explain the tendency that the cool clusters in figure 3 have larger abundances than the hot clusters. Also, Fukazawa et al. (1998) analyzed the X-ray spectra of our sample, excluding the central regions, and found no evidence for the temperature dependence of the iron abundance, which is consistent with our results.

We show the $kT - M_{\text{Fe}}$ relation in figure 4. We also plotted two points for AXJ2019 as described above. There is no clear difference between the clusters at $z < 0.1$ and $0.1 < z < 1.0$. Furthermore AXJ2019 is also consistent with

the other clusters, although its ICM mass may be extremely low. This is because the extremely high abundance compensates for the low gas mass.

Figure 5 shows the $kT - M_{\text{tot}}$ relation. There is no clear difference between the clusters at $z < 0.1$ and $0.1 < z < 1.0$. The most distant cluster AXJ2019 is consistent with the other clusters, while the ICM may be less massive than the other clusters. This may indicate that the formation of the gas halo and the dark matter halo in cluster is not a simultaneous process, and the gas accumulation process continues after the dark matter halo formation is completed.

These data show that there are no differences between the clusters at $z < 0.1$ and $0.1 < z < 1.0$. The most distant cluster at $z = 1.0$, AXJ2019, may be different from the other clusters at $z < 1.0$ in terms of the $kT - M_{\text{gas}}$ and $kT - A_{\text{Fe}}$ relations, although we should note that there is still room to allow AXJ2019 to be consistent with the other clusters by taking its large errors into account. This may suggest that the formation of the gravitational potential well by the dark matter and the metal injection process from galaxies to the ICM had been already finished before $z \sim 1.0$, but the gas accretion process in which the primordial gas falls into the cluster gravitational potential was going on at $z \sim 1.0$. To confirm it, we need the deep observations of X-ray clusters at $z > 1.0$, which will be obtained with forthcoming observatories such as XMM, Chandra, ASTRO-E. It may also be possible that the ASCA results of AXJ2019 (Hattori et al. 1997), particularly about its metallicity, may be in error. For example, the detected iron line may come from a foreground or background AGN. This will also be clarified by future observations.

4. Summary

We analyzed the ASCA data for 29 nearby clusters ($z < 0.1$) and derived temperatures, iron abundances, and X-ray luminosities. Furthermore, we fit the ASCA images, and then determined the best-fit β model parameters for the ICM distribution. These results give the largest and most homogeneous dataset about the ICM distribution obtained with ASCA so far. We compare these results with distant clusters whose temperatures, iron abundances, and luminosities were also measured with ASCA. We found that there is no significant difference between the clusters at $z < 0.1$ and $0.1 < z < 1.0$ in the $kT - L_X$, $kT - M_{\text{gas}}$, $kT - A_{\text{Fe}}$, $kT - M_{\text{Fe}}$, and $kT - M_{\text{tot}}$ relations. However, the most distant cluster in our sample, AXJ2019 at $z = 1.0$, may have different characteristics; its ICM mass may be significantly low, while its metallicity is quite large. They compensate for each other and result in the iron mass which is similar with the other clusters at $z < 1.0$. This may suggest a hint for the evolution of clusters of galaxies

and that the formation of the potential well and the metal injection process of the ICM had finished before $z \sim 1.0$, while the accretion process of the primordial gas was going on at $z \sim 1.0$. However, it is also possible that AXJ2019 is consistent with the other clusters taking its large errors into account.

We would like to thank the ASCA team members for their support. We are also grateful to K. Koyama for helpful discussion and useful comments. HM is supported by the JSPS Postdoctoral Fellowships for Research Abroad.

Reference

- Anders E., Grevesse, N. 1989, *Geochim. Cosmochim. Acta.* 53, 197
- Donahue M., Vorr G. M., Gioia I., Luppino G., Hughes J. P., Stocke J. T. 1998, *ApJ* 502, 550
- Fukazawa Y. 1997, PhD Thesis, The University of Tokyo
- Fukazawa Y., Makishima K., Tamura T., Ezawa H., Xu H., Ikebe Y., Kikuchi K., Ohashi T. 1998, *PASJ* 50, 187
- Furuzawa A., Tawara Y., Kunieda H., Yamashita K., Sonobe T., Tanaka Y., Mushotzky R. 1998, *ApJ* 504, 35
- Hattori M., Ikebe Y., Asaoka I., Takeshima T., Böhringer H., Mihara T., Neumann D. M., Schindler S., Tsuru T., Tamura T. 1997, *Nature* 388, 146
- Hattori M., Matuzawa H., Morikawa K., Kneib J.-P., Yamashita K., Watanabe K., Böhringer H., Tsuru T. G. 1998, *ApJ* 503, 593
- Henry J. P., Henriksen M. J. 1986, *ApJ* 301, 689
- Hughes J. P., Birkinshaw M., Huchra J. P. 1995, *ApJ* 448, L93
- Markevitch M., Yamashita K., Furuzawa A., Tawara Y. 1994, *ApJ* 436, L71
- Markevitch M., Mushotzky R., Inoue H., Yamashita K., Furuzawa A., Tawara Y. 1996, *ApJ* 456, 437
- Masai K. 1984, *Astrophys. Space Science* 98, 367
- Matsuura M., Miyoshi S. J., Yamashita K., Tawara Y., Furuzawa A., Lasenby A. N., Saunders R., Jones M., Hatsukade I. 1996, *ApJ* 466, L75
- Mohr J. J., Mathiesen B., Evrard A. E. 1999, *ApJ* 517, 627
- Mushotzky R. F., Loewenstein M. 1997, *ApJ* 481, L63
- Mushotzky R. F., Scharf C. A. 1997, *ApJ* 482, L13
- Sarazin C. 1986, *Rev. Mod. Phys.* 58, 1
- Schindler S., Hattori M, Neumann D. M., Böhringer H. 1997, *A&A* 317, 646
- Takahashi T., Markevitch M., Fukazawa Y., Ikebe Y., Ishisaki Y., Kikuchi K., Makishima K., Tawara Y., ASCA Image analysis working group 1995, *ASCA News No.3*, p34
- Tanaka Y., Inoue H., Holt S. S. 1994, *PASJ* 46, L37
- Tsuru T., Koyama K., Hughes J. P., Arimoto N., Kii T., Hattori M. 1996, in *UV and X-ray Spectroscopy of Astrophysical and Laboratory Plasmas*, ed. K. Yamashita, T. Watanabe (Universal Academy Press, Inc., Tokyo)

No.]

9

p375

White D. A., Jones C., Forman W. 1997, MNRAS 292, 419

Figure Caption

Fig. 1. Temperature – Luminosity relation. The luminosity is measured in the 2 – 10 keV band. Dots, and triangles denote clusters at $z < 0.1$, $0.1 < z < 1.0$, and AXJ2019 ($z = 1.0$) is denoted by a star.

Fig. 2. Temperature – ICM mass relation. The integration radius for the ICM mass is 1 Mpc from the cluster center. The symbols are the same as in figure 1.

Fig. 3. Temperature – iron abundance relation. The symbols are the same as in figure 1.

Fig. 4. Temperature – iron mass relation. The integration radius for the iron mass is 1.0 Mpc from the cluster center. The symbols are the same as in figure 1.

Fig. 5. Temperature – total mass relation. The integration radius for the total mass is 1.0 Mpc from the cluster center. The symbols are the same as in figure 1.

Table 1. Nearby cluster samples and results of the spectral analysis.

Name	$L_{X(2-10\text{keV})}^{\dagger}$ 10^{44}erg/s	kT keV	A_{Fe} solar	N_{H} 10^{20}cm^{-2}
Ophiuchus	20	10.0 ± 1.5	0.31 ± 0.03	28.0 ± 1.1
A478	16	6.40 ± 0.25	0.35 ± 0.03	20.9 ± 3.7
A2319	15	9.50 ± 0.57	0.23 ± 0.05	5.8 ± 2.6
Tri Aust	12	9.86 ± 0.57	0.23 ± 0.05	14.6 ± 2.5
Perseus	11	5.66 ± 0.12	0.43 ± 0.02	2.9 ± 1.9
A1795	8.2	5.68 ± 0.11	0.38 ± 0.03	0.0 ± 3.0
Coma	7.6	8.95 ± 0.25	0.33 ± 0.05	0.0 ± 0.30
A2256	7.2	7.10 ± 0.28	0.28 ± 0.04	2.7 ± 2.1
A85	7.7	5.88 ± 0.19	0.43 ± 0.04	1.5 ± 2.0
A3571	6.6	7.24 ± 0.24	0.35 ± 0.03	3.0 ± 1.7
A3558	5.0	5.67 ± 0.26	0.29 ± 0.05	2.6 ± 2.9
Hydra-A	3.3	3.71 ± 0.14	0.39 ± 0.06	0.6 ± 3.0
A2199	2.5	4.22 ± 0.06	0.38 ± 0.04	0.0 ± 2.0
A496	2.0	3.98 ± 0.10	0.45 ± 0.04	3.2 ± 1.9
A119	1.8	6.14 ± 0.37	0.35 ± 0.07	1.4 ± 3.4
MKW3s	1.5	3.46 ± 0.14	0.38 ± 0.07	2.0 ± 3.6
2A0335+096 ...	1.7	3.00 ± 0.09	0.48 ± 0.06	11.8 ± 5.3
AWM7	1.2	3.74 ± 0.11	0.55 ± 0.06	9.5 ± 2.6

Table 1. Continued.

Name	$L_{\text{X}(2-10\text{keV})}^{\dagger}$ 10^{44}erg/s	kT keV	A_{Fe} solar	N_{H} 10^{20}cm^{-2}
A2063	1.0	3.72 ± 0.11	0.26 ± 0.07	0.0 ± 3.5
A2147	0.91	4.88 ± 0.22	0.36 ± 0.06	1.6 ± 3.0
A2634	0.52	3.58 ± 0.19	0.29 ± 0.08	1.0 ± 4.2
Centaurus	0.53	3.52 ± 0.09	0.68 ± 0.06	3.5 ± 2.3
A539	0.42	3.27 ± 0.16	0.25 ± 0.08	6.7 ± 4.3
A1060	0.21	3.15 ± 0.08	0.43 ± 0.05	4.9 ± 2.5
AWM4	0.18	2.28 ± 0.03	0.33 ± 0.13	2.3 ± 5.4
A400	0.18	2.54 ± 0.12	0.33 ± 0.10	1.2 ± 4.5
A262	0.20	2.21 ± 0.08	0.33 ± 0.10	4.2 ± 4.4
Virgo	0.16	2.28 ± 0.03	0.55 ± 0.04	7.2 ± 2.8
MKW4s	0.065	2.19 ± 0.21	0.41 ± 0.26	2.1 ± 9.7

Errors are at 90% confidence level.

† Luminosity in the 2 – 10 keV band.

Table 2. Results of the imaging analysis.

Name	β	r_{core}		$n(0)^{\dagger}$ 10^{-3}cm^{-3}	$M_{\text{gas}}^{\ddagger}$ $10^{13}M_{\odot}$	M_{Fe}^{\ddagger} $10^{10}M_{\odot}$	$M_{\text{tot}}^{\ddagger}$ $10^{14}M_{\odot}$
		arcmin	kpc				
Ophiuchus	0.60 ± 0.05	3.50 ± 0.50	227	8.0 ± 1.6	14.6	8.8	6.4
A478	0.70 ± 0.05	1.00 ± 0.25	154	17.0 ± 3.0	11.6	7.9	4.9
A2319	0.55 ± 0.05	2.75 ± 0.75	271	4.6 ± 0.9	12.5	5.6	5.5
Tri Aust	0.60 ± 0.05	3.00 ± 0.50	252	5.1 ± 1.0	10.9	4.9	6.3
Perseus	0.45 ± 0.05	1.25 ± 0.50	40	31.0 ± 6.0	10.0	8.4	2.9
A1795	0.65 ± 0.05	1.25 ± 0.25	135	13.0 ± 3.0	8.5	6.3	4.1
Coma	0.75 ± 0.05	10.25 ± 0.50	416	2.8 ± 0.6	8.9	5.7	6.5
A2256	0.75 ± 0.05	4.50 ± 0.50	457	2.6 ± 0.5	9.4	5.2	5.0
A85	0.60 ± 0.05	1.75 ± 0.50	173	7.4 ± 1.5	8.9	7.5	3.9
A3571	0.60 ± 0.05	2.50 ± 0.50	171	6.7 ± 1.3	7.9	5.4	4.8
A3558	0.50 ± 0.05	1.75 ± 0.50	150	5.2 ± 1.0	7.5	4.3	3.1
Hydra-A	0.60 ± 0.05	0.75 ± 0.50	71	20.0 ± 8.0	5.5	4.2	2.5
A2199	0.60 ± 0.05	1.50 ± 0.50	80	14.0 ± 3.0	4.8	3.5	2.8
A496	0.55 ± 0.05	1.25 ± 0.50	70	13.0 ± 3.0	4.7	4.2	2.5
A119	0.60 ± 0.05	6.00 ± 0.50	462	0.98 ± 0.20	4.6	3.2	3.4
MKW3s	0.65 ± 0.05	1.25 ± 0.30	95	11.0 ± 2.0	3.9	2.9	2.5
2A0335+096	0.60 ± 0.05	0.75 ± 0.25	46	30.0 ± 6.0	3.9	3.7	2.0
AWM7*	0.55 ± 0.05	4.00 ± 1.00	125	4.6 ± 0.9

Table 2. Continued.

Name	β	r_{core}		$n(0)^\dagger$ 10^{-3}cm^{-3}	M_{gas}^\ddagger $10^{13} M_\odot$	M_{Fe}^\ddagger $10^{10} M_\odot$	M_{tot}^\ddagger $10^{14} M_\odot$
		arcmin	kpc				
A2063	0.60 ± 0.05	2.25 ± 0.50	133	4.8 ± 1.0	3.8	1.9	2.5
A2147	0.50 ± 0.05	3.50 ± 0.50	218	1.5 ± 0.3	3.6	2.5	2.6
A2634	0.50 ± 0.05	4.50 ± 1.20	246	1.1 ± 0.2	3.0	1.7	1.9
Centaurus*	0.50 ± 0.05	4.00 ± 0.50	75	5.5 ± 1.1
A539	0.60 ± 0.05	3.50 ± 0.50	164	2.5 ± 0.5	2.8	1.4	2.2
A1060*	0.55 ± 0.05	4.00 ± 1.00	80	4.4 ± 0.9
AWM4	0.55 ± 0.05	1.25 ± 1.20	68	5.1 ± 2.1	1.8	1.1	1.4
A400*	0.45 ± 0.05	2.50 ± 0.80	102	2.1 ± 0.4
A262*	0.50 ± 0.05	2.25 ± 0.75	63	5.5 ± 1.1
Virgo*	0.40 ± 0.05	2.00 ± 1.00	14	19.0 ± 8.0
MKW4s*	0.40 ± 0.05	1.00 ± 0.50	47	2.7 ± 1.1

Errors are at 90% confidence level.

† The central proton density.

‡ Mass within the radius of 1 Mpc from cluster center.

* Gas and iron masses are not listed here, because the FOV of GIS can cover only small region with radii smaller than 1 Mpc from cluster center.

Table 3. Distant cluster samples

Name	z	$L_{X(2-10\text{keV})}^{\dagger}$ 10^{44}erg/s	kT keV	A_{Fe} solar	M_{gas}^{\dagger} $10^{13}M_{\odot}$	M_{Fe}^{\dagger} $10^{10}M_{\odot}$	M_{tot}^{\dagger} $10^{14}M_{\odot}$	Reference*
A1413	0.1430	13	6.72 ± 0.26	0.29 ± 0.05	7.4	4.2	8.9	j, k, m
A2204	0.1530	33	8.47 ± 0.42	j
A1204	0.1700	6.3	3.83 ± 0.19	0.35 ± 0.07	7.0	4.8	3.0	j, k, i
A2218	0.1710	9.4	7.04 ± 0.97	0.18 ± 0.07	j, k
A586	0.1710	8.3	6.61 ± 1.15	j
A1689	0.1800	30	9.02 ± 0.40	0.26 ± 0.06	12.7	6.5	9.6	j, k, m
A1246	0.1870	8.3	6.28 ± 0.54	0.22 ± 0.08	7.8	3.4	5.1	j, k, m
A1763	0.1870	15	8.98 ± 1.02	0.26 ± 0.09	10.7	5.4	5.6	j, k, m
MS0440	0.1900	3.9	5.3 ± 1.3	j
MS0839	0.1940	4.0	4.19 ± 0.36	j
A773	0.1970	13	9.66 ± 1.03	0.24 ± 0.08	j, k
A520	0.2010	16	8.59 ± 0.93	0.25 ± 0.20	j, k
A2163	0.2010	16	12.7 ± 2.0	0.38 ± 0.13	14.9	11.6	12.6	j, h, g, m
A963	0.2060	8.9	6.76 ± 0.44	0.29 ± 0.08	j, k
A1704	0.2190	6.3	4.51 ± 0.56	j
A2219	0.2280	33	11.77 ± 1.26	0.25 ± 0.07	j, k
A2390	0.2300	22	8.90 ± 0.97	0.22 ± 0.06	11.2	4.8	8.3	j, k, m
MS1305+29	0.2410	0.89	2.98 ± 0.52	j
A1835	0.2520	45	8.15 ± 0.46	0.32 ± 0.05	j, k
MS1455	0.2580	12	5.45 ± 0.29	0.33 ± 0.08	j, k
A1758N	0.2800	17	10.19 ± 2.29	j
A483	0.2830	3.3	6.87 ± 1.59	j
ZW3146	0.2900	27	6.35 ± 0.37	0.24 ± 0.05	j, k
MS1008-12	0.3010	6.9	7.29 ± 2.45	j
AC118	0.3080	25	12.08 ± 1.42	0.23 ± 0.09	j, k
MS2137	0.3130	10	4.37 ± 0.38	0.41 ± 0.12	j, k
A1995	0.3180	13	10.70 ± 2.50	j
MS0353-36	0.3200	7.5	8.13 ± 2.57	j

Table 3. Continued.

Name	z	$L_{\text{X}(2-10\text{keV})}^{\dagger}$ 10^{44}erg/s	kT keV	A_{Fe} solar	$M_{\text{gas}}^{\ddagger}$ $10^{13}M_{\odot}$	M_{Fe}^{\ddagger} $10^{10}M_{\odot}$	$M_{\text{tot}}^{\ddagger}$ $10^{14}M_{\odot}$	Reference*
A1722	0.3270	8.3	5.87 ± 0.51	0.25 ± 0.11	j, k
MS1358	0.3270	7.6	6.50 ± 0.68	0.27 ± 0.10	j, k
A959	0.3530	11	6.95 ± 1.85	j
MS1512+36	0.3720	3.7	3.57 ± 1.33	j
A370	0.3730	14	7.13 ± 1.05	j
A851	0.4100	5.8	6.7 ± 2.7	j
RXJ1347-114 ..	0.4510	88	11.37 ± 1.10	0.33 ± 0.10	20.0	12.9	5.8	j, k, l
3C295	0.4600	9.1	7.13 ± 2.06	...	5.3	...	5.7	j, e
MS0451-03	0.5390	19	10.17 ± 1.55	0.16 ± 0.12	j, k
CL0016	0.5410	14	8.0 ± 1.0	0.11 ± 0.12	6.1	j, b, f
CL2236-94	0.552	4.9	6.1 ± 2.6	$0.00 (< 0.38)$	5.8	$0.0 (< 4.3)$	4.4	d
MS1054	0.829	23	12.3 ± 3.1	$0.00 (< 0.25)$	a
AXJ2019+1127	1.00	8.4	8.6 ± 4.2	$1.7_{-0.7}^{+1.3}$	2.4 (4.5) [§]	8.0 (15.1) [§]	3.6 (8.5) [§]	c

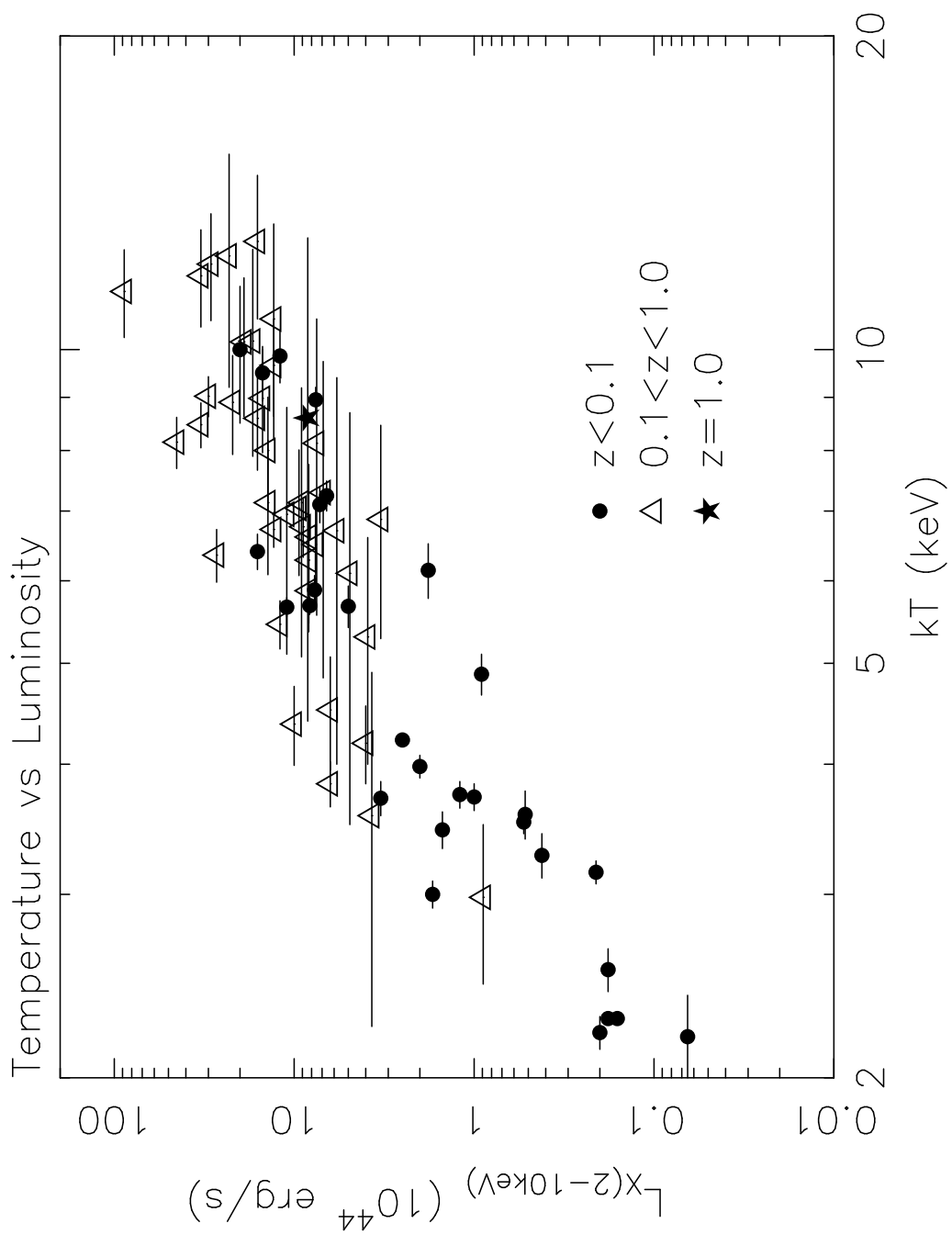
Errors are at 90% confidence level except for AXJ2019. The errors for AXJ2019 are at 1σ level.

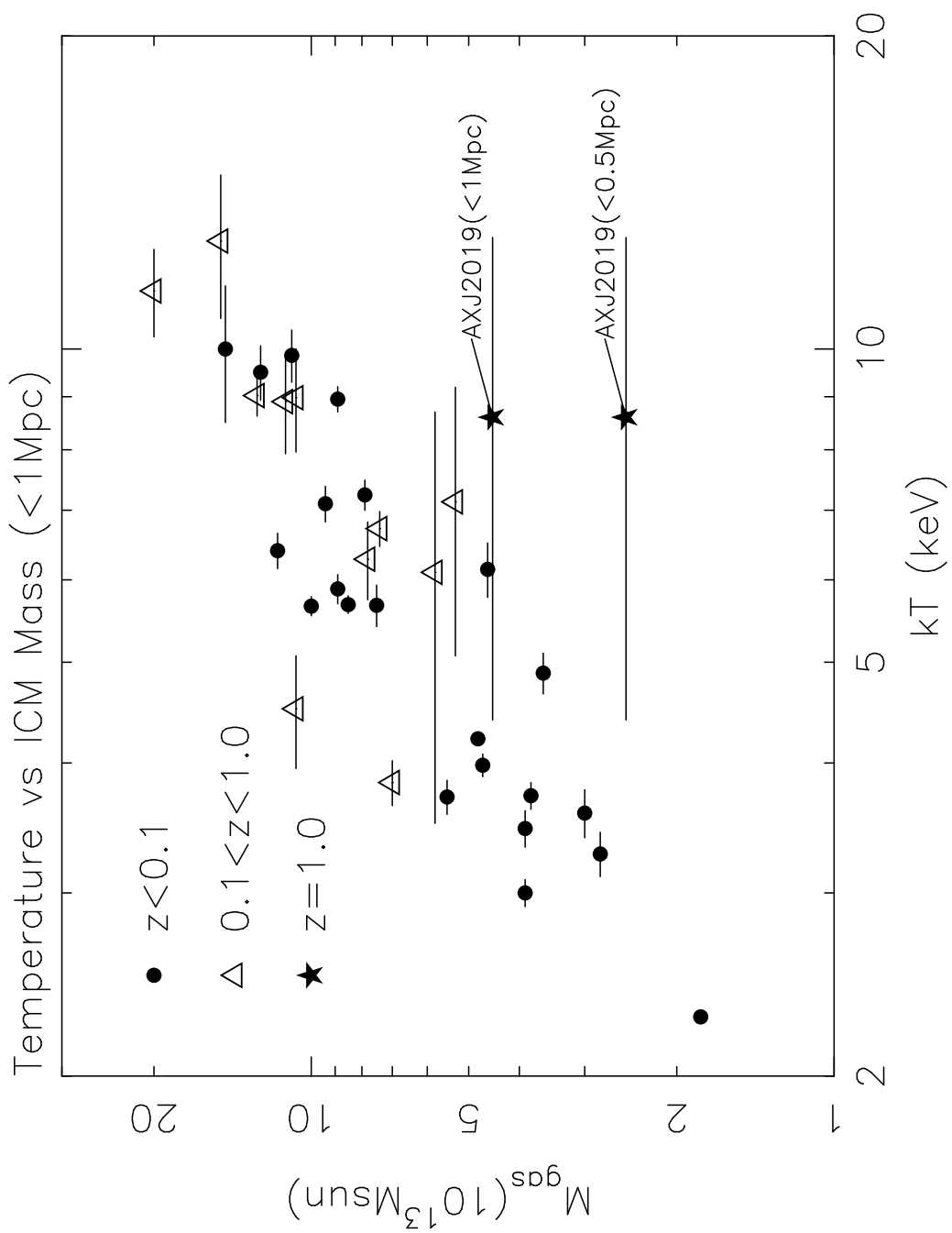
[†] Luminosity in the 2 – 10 keV band.

[‡] Mass within the radius of 1 Mpc from the cluster center.

[§] The ICM in AXJ2019 was detected only within 0.5 Mpc from the center. The values in parenthesis are masses within 1.0 Mpc estimated by extrapolating the best-fit β model.

*References; a. Donahue et al. (1998), b. Furuzawa et al. (1998), c. Hattori et al. (1997), d. Hattori et al. (1998), e. Henry, Henriksen (1986), f. Hughes, Birkinshaw, Huchra (1995) g. Markevitch et al. (1994), h. Markevitch et al. (1996), i. Matsuura et al. (1996), j. Mushotzky, Scharf (1997), k. Mushotzky, Loewenstein (1997), l. Schindler et al. (1997), m. White et al. (1997),





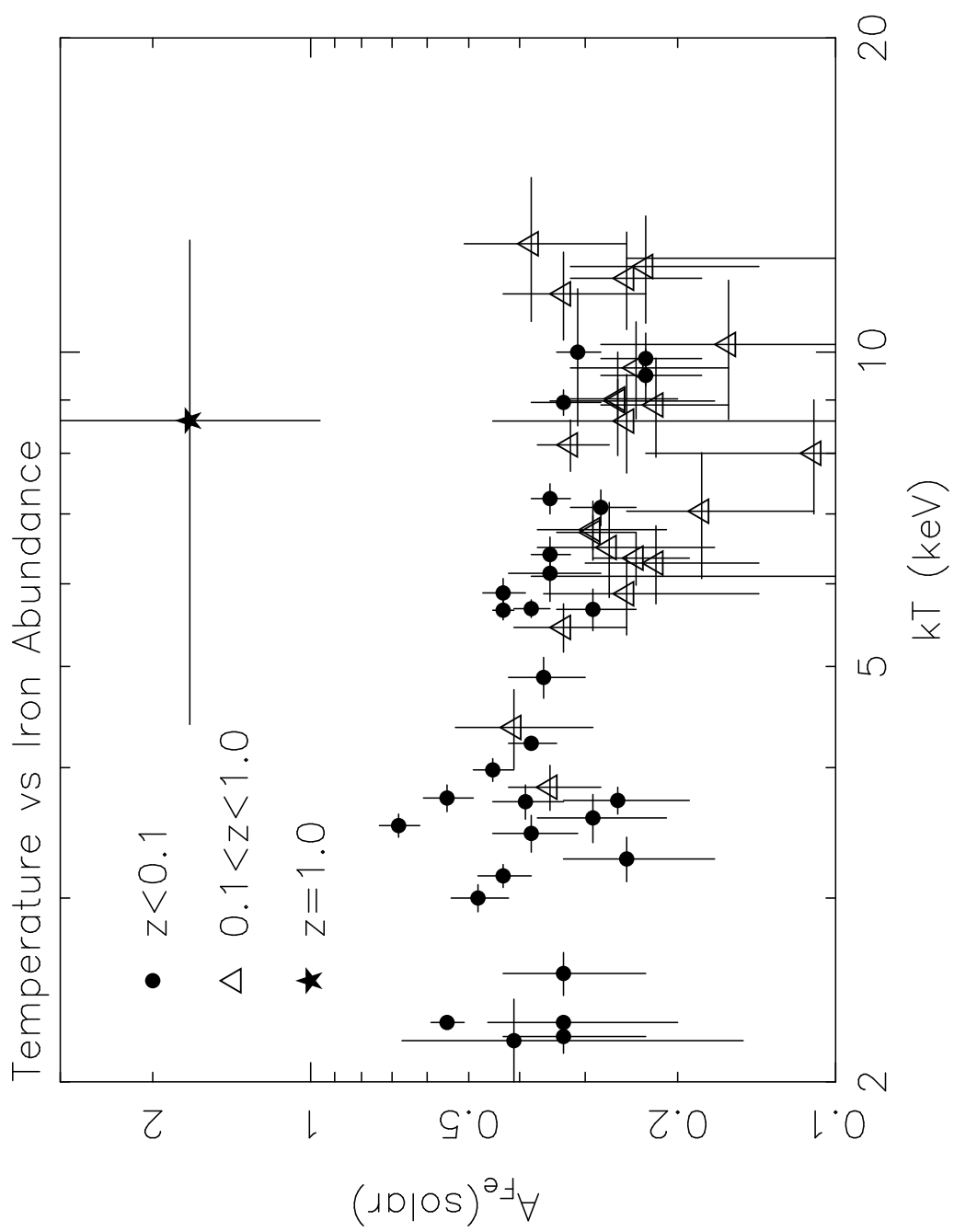


fig4

